Hybrid target design for imprint mitigation in direct-drive inertial confinement fusion

L. Ceurvorst,[1] R. Betti,[2] A. Casner,[1] V. Gopalaswamy,[2] A. Bose,[2] S. X. Hu,[2] E. M. Campbell,[2] S. P. Regan,[2] C. A. McCoy,[3] M. Karasik,[4] J. Peebles,[2] M. Tabak,[5] and W. Theobald[2]

[1]*Université de Bordeaux-CNRS-CEA, CELIA, UMR 5107, F-33405 Talence, France*
[2]*Laboratory for Laser Energetics, University of Rochester, Rochester, New York 14623, USA*
[3]*Sandia National Laboratories, Albuquerque, New Mexico 87185, USA*
[4]*Plasma Physics Division, Naval Research Laboratory, Washington, DC 20375, USA*
[5]*Lawrence Livermore National Laboratory, Livermore, California 94551, USA*

(Received 5 July 2019; revised manuscript received 1 February 2020; accepted 13 May 2020; published 30 June 2020)

A target design for mitigating the Rayleigh-Taylor instability is proposed for use in high energy density and direct-drive inertial confinement fusion experiments. In this scheme, a thin gold membrane is offset from the main target by several-hundred microns. A strong picket on the drive beams is incident upon this membrane to produce x rays which generate the initial shock through the target. The main drive follows shortly thereafter, passing through the ablated shell and directly driving the main target. The efficacy of this scheme is demonstrated through experiments performed at the OMEGA EP facility, showing a reduction of the Rayleigh-Taylor instability growth which scales exponentially with frequency, suppressing development by at least a factor of 5 for all wavelengths below 100 μm. This results in a delay in the time of target perforation by $\sim$40%.

DOI: 10.1103/PhysRevE.101.063207

I. INTRODUCTION

The Rayleigh-Taylor (RT) instability is one of the most ubiquitous hydrodynamic instabilities, forming at the interface of a heavy and a light fluid when the lighter fluid pushes against the heavier fluid. It plays a crucial role in astrophysics, where it is seen in phenomena such as supernovae explosions [1,2], as well as in inertial confinement fusion (ICF) [3–5]. In ICF, as mass ablates off of the surface of a target, a light, hot plasma forms which accelerates the remainder of the target inward. This interface experiences the instability in a form known as ablative RT instability (aRTI) [6–9].

The evolution of the aRTI strongly depends on the initial perturbations imparted both by target manufacturing defects [10] and by the nonuniformities in the driver beam [11]. When a beam impinges directly on a target, the modulations of the laser beam's intensity imprint onto the target, creating the mass-density perturbations which seed the RT instability. To minimize these seed amplitudes, many experiments are run in indirect drive [12–16]. In this scheme, rather than focusing the beams directly onto a target, a high-Z layer is irradiated to convert the laser energy into x rays. These x rays are used as the target driver, providing much smoother irradiation due to their incoherence [17]. However, once the conduction zone of the target—the region between the laser-deposition and ablation fronts—has developed, pressure perturbations with wavelengths less than the zone's width are suppressed by thermal smoothing [18]. As a result, the level of smoothing produced by indirect drive is no longer required, making the conversion to x rays wasteful [19].

To avoid sacrificing efficiency, a wide variety of designs have been developed to mitigate the laser imprint onto the target surface. Much work has gone into improving the laser drives, including smoothing the beam profiles using phase plates [20–22], smoothing by spectral dispersion (SSD) [23], induced spatial incoherence [24], multifrequency modulators [25], and designing the beams' temporal profiles to shape the adiabat of the shell [26–29]. Other research focuses on target design using foam layers [30–33], high-Z dopants in the ablated region [34], or preheating the target surface [35,36]. While all of these designs reduce RTI growth, none have yet proven sufficient for suppressing it to the levels required for high-performance implosions.

In this paper, the performance of a proposed concept is explored which takes advantage of the smoothness of indirect drive and the efficiency of direct drive. This hybrid scheme uses soft x rays only to drive the first shock, while direct illumination implodes the capsule. Another previous technique uses a high-Z coating preheated by a low-level laser or x-ray prepulse to create sufficient standoff for smoothing [37–39]. The design proposed herein eliminates the need for preheating and removes the high-Z layer from contact with the target entirely. To do so, a target is surrounded by a thin (less than 1 μm) CH membrane that is externally coated with a tens-of-nm-thick layer of Au. The membrane is offset by several-hundred microns from the target's surface. Figure 1 shows a schematic of the design in planar geometry. The target is driven using a picketed laser pulse in a direct-drive configuration. The high-intensity picket impinges on the membrane, producing incoherent x-ray radiation. These x rays form a smooth radiation flash which serves as the initial seed on the main target surface and drives the first shock through the target. This shock sets up the conduction zone of the target over several-hundred picoseconds. The main pulse passes through the now-underdense membrane plasma and directly drives the target. Since the conduction zone was already established by the x rays, perturbations in the main

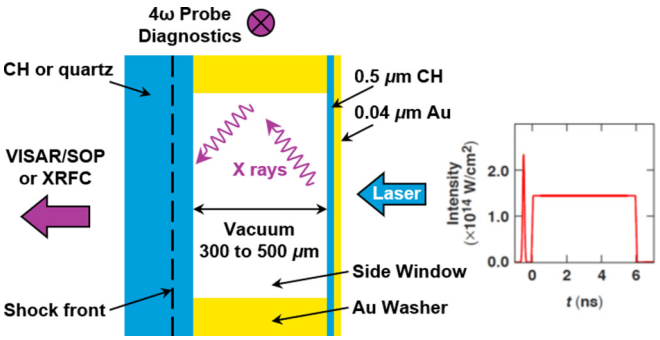

FIG. 1. Schematic of the hybrid direct-drive target design in planar geometry.

pulse's profile whose wavelength is less than the conduction zone's width will be exponentially smoothed [18], and only the longest wavelengths will grow via the aRTI. The proof-of-concept experiment described herein was performed at the OMEGA EP laser [40].

II. X-RAY-DRIVEN SHOCKS

Figure 1 shows the experimental configuration. An Au washer with a 1.5 mm outer diameter, 20 μm wall thickness, and 300 μm or 500 μm height was glued on a planar quartz or polystyrene target. The height of the washer determined the standoff distance of a 0.5-μm-thick CH membrane from the target plane. The membrane was coated with a ~40 nm layer of Au. The area between the target and the membrane was held at vacuum. The Au side was irradiated with one ultraviolet (UV) beam ($\lambda = 351$ nm) equipped with a distributed phase plate, creating a flat-top spatial intensity profile which is well described by an eighth-order super-Gaussian with a 750 μm diameter.

The first phase of this experiment aimed to show that a shock can be generated solely by the x rays produced via the interaction of the picket pulse with the Au membrane. The pressure measurements used 140-μm-thick quartz foils that were coated with a 100 nm Al layer on the washer side and with an antireflection (AR) coating for $\lambda = 532$ nm on the backside. The Au washer was either 300 μm or 500 μm thick, which will be referred to as the "Hybrid300" and "Hybrid500" targets, respectively. A picket pulse with a 150 ps duration and an intensity of 1–2 $\times$ 10^{14} W cm^{-2} interacted with the Au coating to generate the x-ray pulse that drove the shock wave in the planar target. No long pulse followed, meaning that the evolution seen here is solely due to the picket pulse's interaction with the thin membrane. The Au washer serves not only to displace the membrane but also to provide some containment of the x-ray energy. The propagation of the shock wave in the main target was observed with a velocity interferometer system for any reflector (VISAR) [41] and a streaked optical pyrometer (SOP) [42]. Time-resolved measurements of the shock velocity and shock-front emission were provided by VISAR and SOP, respectively. The shock pressure was then inferred from the shock velocity using the fit to the quartz principal Hugoniot [43].

Figure 2(a) shows a characteristic VISAR image of a Hybrid300 target. Note that at early times, the optical diagnostic

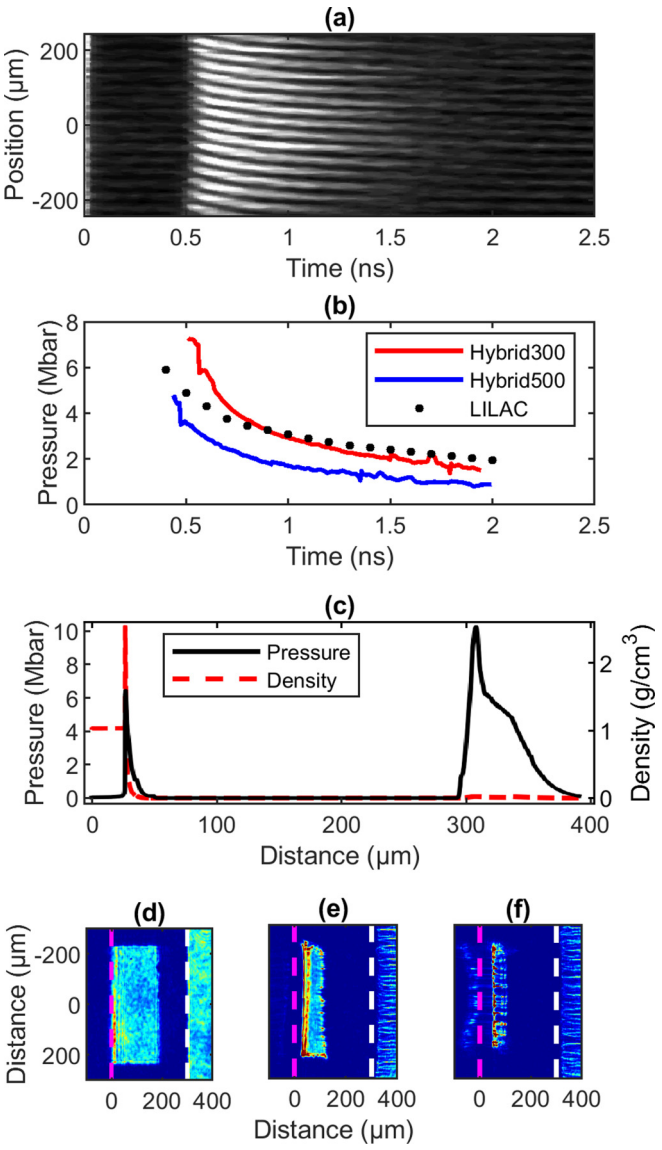

FIG. 2. (a) VISAR image of the Hybrid300 target. (b) Experimentally inferred pressure evolution of shock waves that were created by the x-ray flash. 1D LILAC simulations of the Hybrid300 target (black dotted line) show approximate agreement with the experimental data. (c) LILAC simulations of the Hybrid300 target showing pressure and density as a function of longitudinal position at $t = 200$ ps. (d)–(f) Radiographs showing the transmission of the 4ω optical probe through the washer's side window, (d) before the drive begins, (e) at $t = 380$ ps, and (f) at $t = 450$ ps. The superimposed vertical dashed lines show the target's original surface (magenta, left) and the high-Z membrane's initial location (white, right). The pulse is incident from the right.

blanked due to free charge carriers produced by the x-ray pulse [44]. This limited the subsequent analysis to times after $t \approx 0.5$ ns. The resulting pressure evolution of the shock waves for both the Hybrid300 and Hybrid500 targets inferred from these images is shown in Fig. 2(b). The measurements show that a rapidly decaying shock wave with Mbar-scale initial pressures was created shortly after the interaction of the picket pulse with the high-Z membrane. One-dimensional

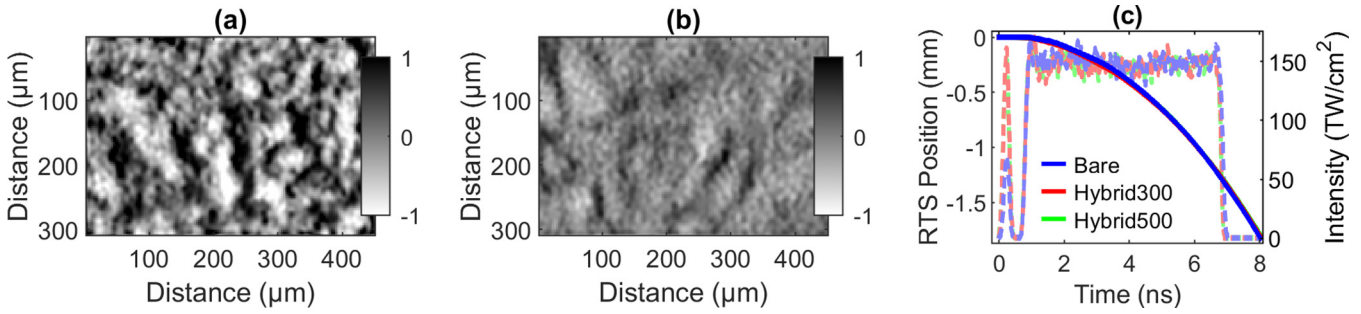

FIG. 3. Optical depth images of (a) a bare target and (b) a Hybrid300 target after ∼ 4.2 ns. (c) LILAC-simulated trajectories (solid line) of the rear target surface (RTS) for each target using realistic laser profiles (dashed faded line).

(1D) hydrodynamic simulations with the LILAC code [45] of the Hybrid300 targets predict similar pressures by an x-ray–driven shock. The lower pressure in Hybrid500 targets compared to Hybrid300 targets is due to increased losses resulting from a larger hohlraum. Due to the 1D nature of the code, these geometric losses are not taken into account, and the LILAC simulations of the Hybrid500 targets are identical to the Hybrid300 results.

Pressure and density profiles from a simulated Hybrid300 target are shown in Fig. 2(c) at $t = 200$ ps as the shock is generated. The simulations show an unsupported shock that rapidly decays while expanding plasmas from both the target and the exploding membrane fill the vacuum. The region between both plasma fronts remained at vacuum while these shocks formed, indicating that they were generated by x rays. Both low-density expanding plasmas collide at ∼500 ps near the center. This was experimentally confirmed by using an Au washer with an opening that provided a clear path for a 263 nm, 10 ps optical probe laser [46] that propagated perpendicularly to the target axis. By firing the optical probe laser at different time delays with respect to the x-ray pulse in subsequent shots, this probing enabled the observation of the plasma expansion between both foils. As shown in Figs. 2(d)–2(f), a clear gap between both colliding plasmas was observed for a probe time of up to 380 ps, while at a probe delay of 450 ps, the probe beam was almost completely absorbed. This indicates the two plasmas collided between 380 ps and 450 ps, in agreement with the hydrodynamic simulations. This measurement, together with the pressure measurements, shows that the shock was indeed generated by the x-ray flash and not by material from the exploding membrane. The simulations show that the shock collision generates a weaker shock that catches up with the initial shock front only after several nanoseconds, well after the observation time in Fig. 2(b). As such, this rebounding shock does not influence the observations made here, and the shock pressures are solely due to the x-ray flash.

III. RAYLEIGH-TAYLOR GROWTH COMPARISON

Having established that a multi-Mbar shock is generated by the x-ray flash, a new configuration was deployed to observe the effects that this preconditioning of the target has on imprint and aRTI growth. The imprint shots used a 30-μm-thick planar polystyrene foil that was coated with a 100 nm Al layer on the washer side and no AR coating. The performance of the hybrid targets was compared to a bare 30-μm-thick polystyrene foil without Au washer. A drive pulse was added after the x-ray-generating picket (see Fig. 1). The picket had an intensity of $0.7 \pm 0.1 \times 10^{14}$ W cm^{-2} when incident on the bare target and $1.8 \pm 0.1 \times 10^{14}$ W cm^{-2} in the case of the hybrid targets. The intensity was increased in the hybrid case so that the x rays created by the picket would generate an initial shock matching the 1D performance of the bare targets as predicted by LILAC simulations [45]. The main 6-ns-long square pulse followed 500 ps later. The total energy was 3.45 ± 0.11 kJ, providing an average on-target intensity of $1.54 \pm 0.09 \times 10^{14}$ W cm^{-2} in the main pulse. The simulated trajectory of the rear surface of each target is shown in Fig. 3(c). As can be seen, the 1D behavior is identical across designs, yielding an acceleration of $g = 35 \pm 3$ μm/ns^2. Therefore, given that the main drive pulses were identical in the bare and hybrid cases, no substantial impact on the drive efficiency is expected from this design.

No SSD was used, causing the beam speckle pattern to serve as three-dimensional, multimode imprint seeds for aRTI. The evolution of aRTI was observed through face-on x-ray radiography [10]. A gated x-ray framing camera (XRFC) [47] with a four-strip microchannel plate (MCP) coupled with a 4×4 array of 10-μm-diameter pinholes was used to image the instability at various times. The x rays for this radiography were produced from a Gd foil with one 2.17 ± 0.27 kJ UV beam. The x-ray emission was filtered by a 6-μm-thick Al foil, which provided quasimonochromatic radiation at ∼1.4 keV. The timing of the backlighting pulse was adjusted to allow different evolution times to be observed between 0.8 ns and 5.7 ns. The images on each strip of the MCP were correlated, Wiener deconvolved, and converted to optical depth (OD) using a third-degree polynomial fit similar to the procedure described in Ref. [48]. Examples of these OD images are shown in Figs. 3(a) and 3(b) at $t = 4.2$ ns for the bare and Hybrid300 targets, respectively. The high-frequency components in Fig. 3(b) are at noise and are the result of photon statistics.

Azimuthally averaged Fourier spectra [49] of the OD modulations at different times are shown in Figs. 4(a) and 4(b) for both the bare and hybrid targets. The uncertainty for each spectrum is approximately 12% across all frequencies. The noise band indicates the range of noise spectra measured between all shots for ease of viewing. Modulation growth

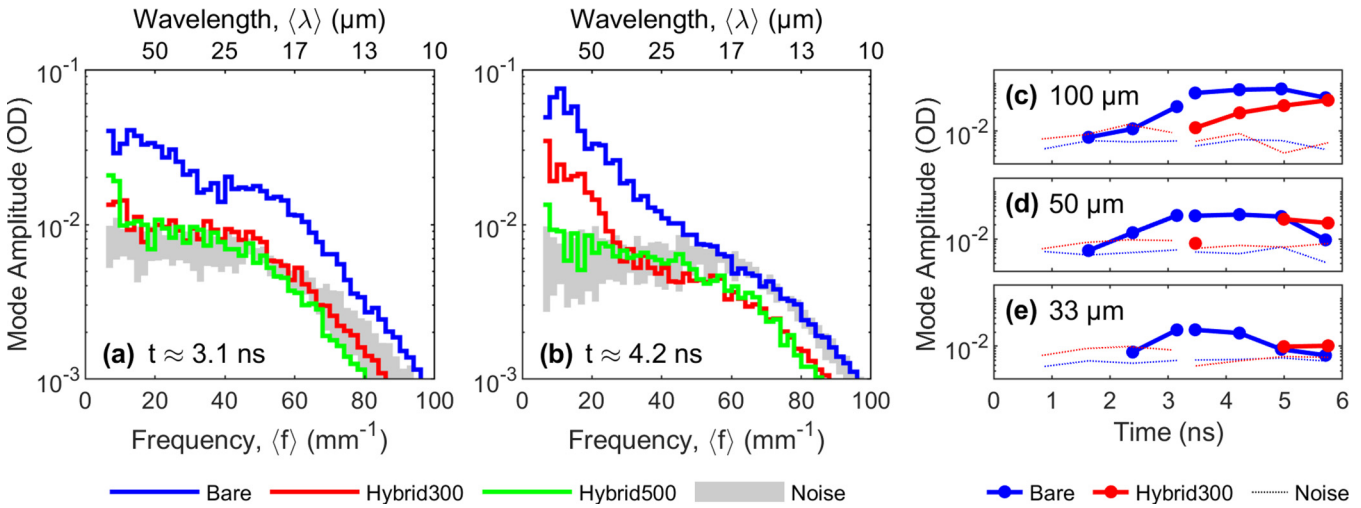

FIG. 4. The azimuthally averaged Fourier spectra of the three targets at (a) 3.1 ns and (b) 4.2 ns. The noise band ranges between the minimum and maximum observed noise levels for the three shots in each subimage. (c)–(e) The evolution of specified wavelengths comparing bare and Hybrid300 targets. The dotted lines represent the noise levels of the corresponding target. Only measurements which exceed noise are shown.

was significantly reduced in both hybrid targets, with the bare targets achieving a peak amplitude of 4.1×10^{-2} OD after just 3.1 ns compared to Hybrid300 reaching a similar level of 2.6×10^{-2} OD after 4.2 ns and only at low frequencies. The Hybrid500 target did not exceed noise until the final observed time of 5.7 ns. However, there were alignment concerns with this target resulting in the signal appearing at the edge of the backlit region. As a result, it has been excluded from the remainder of this discussion.

The evolution of select wavelengths is shown in Figs. 4(c)–4(e). When the growth of the RTI is sufficient to cause a bubble's height to match the target's thickness, perforation will occur, and amplitudes across the spectrum will decrease starting at the higher frequencies. This occurred in the bare targets after 3.8 ± 0.5 ns and possibly in the Hybrid300 targets after 5.3 ± 0.5 ns, thus delaying target decay by at least 40%.

IV. QUANTIFYING IMPRINT MITIGATION

To quantify the imprint mitigation levels, the Hybrid300 spectra must be directly compared to the bare spectra. However, by the time the signal exceeded noise in the hybrid case, the bare target had already perforated. To make these directly comparable, noise was subtracted from each spectrum in quadrature. Then, assuming exponential aRTI growth for the Hybrid300 target, its spectrum at $t = 4.23$ ns was backprojected using the well-known Betti-Takabe growth rate for CH [3], $\gamma = 0.98\sqrt{kg/(1+kL_{\min})} - 1.7kV_a$. Here, $k = 2\pi f/c$ is the wave number, $g = 35 \pm 3\ \mu\text{m/ns}^2$ the acceleration, $V_a = 2 \pm 1\ \mu\text{m/ns}$ the ablation velocity, and $L_{\min} = 10 \pm 1\ \mu\text{m}$ the minimum density scale length, all extracted from the corresponding simulations. This produced an approximate spectrum for the Hybrid300 targets at $t = 3.15$ ns, shown in Fig. 5(a). The level of imprint suppression is then given by the ratio of the projected Hybrid300 spectrum to the bare spectrum; see Fig. 5(b).

The reduction in amplitude roughly follows an exponential decay of e^{-kL}, where $L = 13 \pm 2\ \mu$m. When a conduction zone is formed, it smooths pressure perturbations through thermal smoothing according to e^{-kD_c}, where D_c is the conduction zone width [18]. LILAC Hybrid300 simulations predict this zone width after the x-ray flash and before the main pulse to be $D_c = 16 \pm 3\ \mu$m. Since this zone was formed by a smooth x-ray source in the hybrid cases, minimal imprint will have occurred during its creation and it will instantly smooth any imprint from the main drive. The exponentially reduced

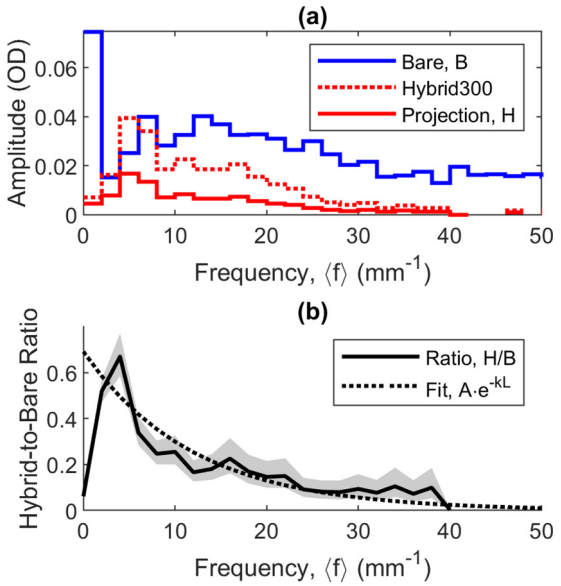

FIG. 5. (a) The Hybrid300 spectrum at $t = 4.23$ ns (dotted line) was backprojected to $t = 3.15$ ns (solid line, bottom) to be directly comparable to the bare spectrum at this time (solid line, top). (b) The ratio of the Hybrid300 projected spectrum to the bare spectrum at 3.15 ns was fitted with an exponential to calculate the smoothing effects. The gray-shaded region represents the uncertainty resulting from the backprojection of the Hybrid300 spectrum.

perturbations observed here are therefore a strong indicator of thermal smoothing. It is worth noting that $D_c \propto I^{4/3}$ [35], so the level of smoothing could potentially be tuned by altering the picket intensity.

V. CONCLUSION

In summary, the performance of the hybrid target design was measured through planar experiments performed at the OMEGA EP facility. Shocks were generated by the x-ray flashes and the growth of the aRTI was significantly reduced, enabling the targets to be driven for at least 40% greater duration through the mitigation of the initial imprinting seed. High-frequency modes were suppressed by a factor $\propto e^{-k13\ \mu\mathrm{m}}$ due to the smooth conduction zone created by the x-ray flashes. These results demonstrate the efficacy of the hybrid scheme and present a promising path forward towards mitigating laser imprint in ICF and high-energy-density research.

ACKNOWLEDGMENTS

This material is based upon work supported by the U.S. Department of Energy National Nuclear Security Administration under Award No. DE-NA0003856, U.S. Department of Energy Grant No. DE-SC0014318, the Enabling Research Grant No. ENR-IFE19.CCFE-01, the University of Rochester, the New York State Energy Research and Development Authority, and Sandia National Laboratories under Contract No. DE-NA0003525 from the National Nuclear Security Administration. Neither the U.S. Government nor any agency thereof makes any warranty or assumes any legal liability or responsibility for the accuracy, completeness, or usefulness of any information disclosed.

[1] K. Kifonidis, T. Plewa, H.-T. Janka, and E. Müller, Astron. Astrophys. **408**, 621 (2003).
[2] W. H. Cabot and A. W. Cook, Nat. Phys. **2**, 562 (2006).
[3] R. Betti, V. N. Goncharov, R. L. McCrory, and C. P. Verdon, Phys. Plasmas **5**, 1446 (1998).
[4] S. P. Regan, R. Epstein, B. A. Hammel, L. J. Suter, H. A. Scott, M. A. Barrios, D. K. Bradley, D. A. Callahan, C. Cerjan, G. W. Collins *et al.*, Phys. Rev. Lett. **111**, 045001 (2013).
[5] A. Casner, C. Mailliet, S. F. Khan, D. Martinez, N. Izumi, D. Kalantar, P. Di Nicola, J. M. Di Nicola, E. Le Bel, I. Igumenshchev *et al.*, Plasma Phys. Control. Fusion **60**, 014012 (2018).
[6] P. Ramaprabhu, G. Dimonte, P. Woodward, C. Fryer, G. Rockefeller, K. Muthuraman, P.-H. Lin, and J. Jayaraj, Phys. Fluids **24**, 074107 (2012).
[7] A. Casner, V. A. Smalyuk, L. Masse, I. Igumenshchev, S. Liberatore, L. Jacquet, C. Chicanne, P. Loiseau, O. Poujade, D. K. Bradley *et al.*, Phys. Plasmas **19**, 082708 (2012).
[8] H. Zhang, R. Betti, R. Yan, D. Zhao, D. Shvarts, and H. Aluie, Phys. Rev. Lett. **121**, 185002 (2018).
[9] D. A. Martinez, V. A. Smalyuk, J. O. Kane, A. Casner, S. Liberatore, and L. P. Masse, Phys. Rev. Lett. **114**, 215004 (2015).
[10] J. P. Knauer, R. Betti, D. K. Bradley, T. R. Boehly, T. J. B. Collins, V. N. Goncharov, P. W. McKenty, D. D. Meyerhofer, V. A. Smalyuk, C. P. Verdon *et al.*, Phys. Plasmas **7**, 338 (2000).
[11] V. A. Smalyuk, O. Sadot, R. Betti, V. N. Goncharov, J. A. Delettrez, D. D. Meyerhofer, S. P. Regan, T. C. Sangster, and D. Shvarts, Phys. Plasmas **13**, 056312 (2006).
[12] J. D. Lindl, P. Amendt, R. L. Berger, S. G. Glendinning, S. H. Glenzer, S. W. Haan, R. L. Kauffman, O. L. Landen, and L. J. Suter, Phys. Plasmas **11**, 339 (2004).
[13] A. Benuzzi, T. Löwer, M. Koenig, B. Faral, D. Batani, D. Beretta, C. Danson, and D. Pepler, Phys. Rev. E **54**, 2162 (1996).
[14] S. D. Rothman, A. M. Evans, P. Graham, C. J. Horsfield, and T. Jalinaud, J. Phys. D: Appl. Phys. **35**, 3021 (2002).
[15] G. Dimonte, D. L. Youngs, A. Dimits, S. Weber, M. Marinak, S. Wunsch, C. Garasi, A. Robinson, M. J. Andrews, P. Ramaprabhu *et al.*, Phys. Fluids **16**, 1668 (2004).
[16] A. Casner L. Masse, S. Liberatore, P. Loiseau, P. E. Masson-Laborde, L. Jacquet, D. Martinez, A. S. Moore, R. Seugling, S. Felker *et al.*, Phys. Plasmas **22**, 056302 (2015).
[17] J. Lindl, Phys. Plasmas **2**, 3933 (1995).
[18] V. N. Goncharov, S. Skupsky, T. R. Boehly, J. P. Knauer, P. McKenty, V. A. Smalyuk, R. P. J. Town, O. V. Gotchev, R. Betti, and D. D. Meyerhofer, Phys. Plasmas **7**, 2062 (2000).
[19] J. L. Kline, S. H. Batha, L. R. Benedetti, D. Bennett, S. Bhandarkar, L. F. Berzak Hopkins, J. Biener, M. M. Biener, R. Bionta, E. Bond *et al.*, Nucl. Fusion **59**, 112018 (2019).
[20] Y. Kato, K. Mima, N. Miyanaga, S. Arinaga, Y. Kitagawa, M. Nakatsuka, and C. Yamanaka, Phys. Rev. Lett. **53**, 1057 (1984).
[21] Y. Lin, G. N. Lawrence, and T. J. Kessler, Opt. Lett. **21**, 1703 (1996).
[22] T. R. Boehly, V. A. Smalyuk, D. D. Meyerhofer, J. P. Knauer, D. K. Bradley, R. S. Craxton, M. J. Guardalben, S. Skupsky, and T. J. Kessler, J. Appl. Phys. **85**, 3444 (1999).
[23] S. Skupsky, R. W. Short, T. Kessler, R. S. Craxton, S. Letzring, and J. M. Soures, J. Appl. Phys. **66**, 3456 (1989).
[24] R. H. Lehmberg, A. J. Schmitt, and S. E. Bodner, J. Appl. Phys. **62**, 2680 (1987).
[25] T. J. B. Collins, J. A. Marozas, K. S. Anderson, R. Betti, R. S. Craxton, J. A. Delettrez, V. N. Goncharov, D. R. Harding, F. J. Marshall, R. L. McCrory *et al.*, Phys. Plasmas **19**, 056308 (2012).
[26] N. Metzler, A. L. Velikovich, A. J. Schmitt, and J. H. Gardner, Phys. Plasmas **9**, 5050 (2002).
[27] N. Metzler, A. L. Velikovich, A. J. Schmitt, M. Karasik, V. Serlin, A. N. Mostovych, S. P. Obenschain, J. H. Gardner, and Y. Aglitskiy, Phys. Plasmas **10**, 1897 (2003).
[28] V. N. Goncharov, J. P. Knauer, P. W. Mckenty, P. B. Radha, T. C. Sangster, S. Skupsky, R. Betti, R. L. McCrory, and D. D. Meyerhofer, Phys. Plasmas **10**, 1906 (2003).
[29] K. Anderson and R. Betti, Phys. Plasmas **11**, 5 (2004).
[30] R. J. Mason, R. A. Kopp, H. X. Vu, D. C. Wilson, S. R. Goldman, R. G. Watt, M. Dunne, and O. Willi, Phys. Plasmas **5**, 211 (1998).
[31] R. G. Watt, J. Duke, C. J. Fontes, P. L. Gobby, R. V. Hollis, R. A. Kopp, R. J. Mason, D. C. Wilson, C. P. Verdon, T. R. Boehly *et al.*, Phys. Rev. Lett. **81**, 4644 (1998).

[32] T. Takeda, K. Mima, T. Norimatsu, H. Nagatomo, and A. Nishiguchi, Phys. Plasmas **10**, 2608 (2003).
[33] B. Delorme, M. Olazabal-Loumé, A. Casner, Ph. Nicolaï, D. T. Michel, G. Riazuelo, N. Borisenko, J. Breil, S. Fujioka, M. Grech *et al.*, Phys. Plasmas **23**, 042701 (2016).
[34] S. X. Hu, G. Fiksel, V. N. Goncharov, S. Skupsky, D. D. Meyerhofer, and V. A. Smalyuk, Phys. Rev. Lett. **108**, 195003 (2012).
[35] T. J. B. Collins and S. Skupsky, Phys. Plasmas **9**, 275 (2002).
[36] J. Badziak, A. Kasperczuk, P. Parys, T. Pisarczyk, M. Rosiński, L. Ryć, J. Wołowski, R. Suchańska, J. Krása, E. Krousky *et al.*, Appl. Phys. Lett. **92**, 211502 (2008).
[37] S. P. Obenschain, D. G. Colombant, M. Karasik, C. J. Pawley, V. Serlin, A. J. Schmitt, J. L. Weaver, J. H. Gardner, L. Phillips, Y. Aglitskiy *et al.*, Phys. Plasmas **9**, 2234 (2002).
[38] M. Karasik, J. L. Weaver, Y. Aglitskiy, J. Oh, and S. P. Obenschain, Phys. Rev. Lett. **114**, 085001 (2015).
[39] M. Karasik, J. Oh, A. J. Schmitt, and S. P. Oberschain (unpublished).
[40] L. J. Waxer, M. J. Guardalben, J. H. Kelly, B. E. Kruschwitz, J. Qiao, I. A. Begishev, J. Bromage, C. Dorrer, J. L. Edwards, L. Folnsbee *et al.*, The OMEGA EP high-energy, short-pulse laser system, in *Conference on Lasers and Electro-Optics/Quantum Electronics and Laser Science Conference and Photonic Applications Systems Technologies*, OSA Technical Digest (CD) (Optical Society of America, 2008), p. JThB1.
[41] P. M. Celliers, D. K. Bradley, G. W. Collins, D. G. Hicks, T. R. Boehly, and W. J. Armstrong, Rev. Sci. Instrum. **75**, 4916 (2004).
[42] M. C. Gregor, R. Boni, A. Sorce, J. Kendrick, C. A. McCoy, D. N. Polsin, T. R. Boehly, P. M. Celliers, G. W. Collins, D. E. Fratanduono *et al.*, Rev. Sci. Instrum. **87**, 114903 (2016).
[43] M. P. Desjarlais, M. D. Knudson, and K. R. Cochrane, J. Appl. Phys. **122**, 035903 (2017).
[44] S. Laffite, S. D. Baton, P. Combis, J. Clerouin, M. Koenig, V. Recoules, C. Rousseaux, and L. Videau, Phys. Plasmas **21**, 082705 (2014).
[45] J. Delettrez, R. Epstein, M. C. Richardson, P. A. Jaanimagi, and B. L. Henke, Phys. Rev. A **36**, 3926 (1987).
[46] D. Haberberger, S. Ivancic, S. X. Hu, R. Boni, M. Barczys, R. S. Craxton, and D. H. Froula, Phys. Plasmas **21**, 056304 (2014).
[47] D. K. Bradley, P. M. Bell, O. L. Landen, J. D. Kilkenny, and J. Oertel, Rev. Sci. Instrum. **66**, 716 (1995).
[48] V. A. Smalyuk, T. R. Boehly, D. K. Bradley, J. P. Knauer, and D. D. Meyerhofer, Rev. Sci. Instrum. **70**, 647 (1999).
[49] V. A. Smalyuk, O. Sadot, J. A. Delettrez, D. D. Meyerhofer, S. P. Regan, and, T. C. Sangster, Phys. Rev. Lett. **95**, 215001 (2005).